2010 HST Calibration Workshop
Space Telescope Science Institute, 2010
Susana Deustua and Cristina Oliveira, eds.

Performance of the Space Telescope Imaging Spectrograph after SM4

Charles R. Proffitt[1], A. Aloisi, R. C. Bohlin, K. A. Bostroem, C. R. Cox, R. I. Diaz, W. V. Dixon[2], P. Goudfrooij, P. Hodge, M. E. Kaiser[2], M. D. Lallo, D. Lennon[3], S. Niemi, R. V. Osten, I. Pascucci[3], E. Smith, sM. A. Wolfe, B. York, W. Zheng[2],

Space Telescope Science Institute, 3700 San Martin Drive, Baltimore MD 21212

T. R. Gull[4], D. J. Lindler[5], and B. E. Woodgate[4]

Goddard Space Flight Center, Greenbelt Maryland 20771

Abstract.

On May 17, 2009, during the fourth EVA of SM4, astronauts Michael Good and Mike Massimino replaced the failed LVPS-2 circuit board on the Space Telescope Imaging Spectrograph (STIS), restoring this *HST* instrument to operation after a nearly 6 year hiatus. STIS after this 2009 repair operates in much the same way as it did during the 2001-2004 period of operations with the Side-2 electronics. Internal and external alignments of the instrument are similar to what they had been in 2004, and most changes in performance are modest. The STIS CCD detector continued to experience radiation damage during the hiatus in operations, leading to decreased charge transfer efficiency (CTE) and an increased number of hot pixels. The sensitivities for most modes are surprisingly close to what was expected from simple extrapolation of the 2003-2004 trends, although the echelle modes show somewhat more complex behavior. The biggest surprise was that the dark count rate for the NUV MAMA detector after SM4 has been much larger than had been expected; it is currently about 2.5 times bigger than it was in 2004 and is only slowly decreasing. We discuss how these changes will affect science with STIS now and in the future.

1. Introduction

STIS was designed as a replacement for the two original *HST* spectrographs, the Goddard High-Resolution Spectrograph and the Faint Object Spectrograph. These previous generation spectrographs had been limited to small 1-D sensors (512 pixel Digicons), while STIS was specifically designed to take advantage of availability of large, sensitive 2-D detector arrays.

STIS is a complex instrument with a large number of modes and options. The instrument includes three independent detectors (see Table 1). While only one of these detectors can be used at any given time, switching between them takes a minimal amount of time,

---

[1]Science Programs, Computer Sciences Corporation

[2]Department of Physics and Astronomy, Johns Hopkins University

[3]European Space Agency

[4]National Aeronautics and Space Administration

[5]Sigma Space Corporation

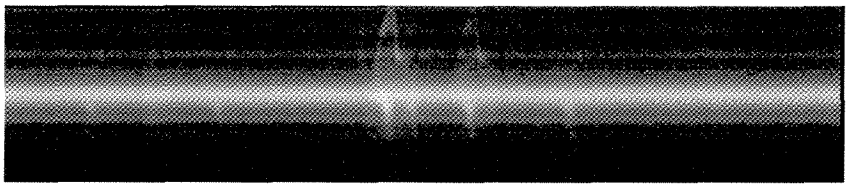

Figure 1: A detail from the STIS Early Release Observation OAC6010D0 of the nebula around the superluminous blue variable star η Car taken in June of 2009, using the 7283 CENWAVE setting of the G750M grating with the 52X0.1 aperture, illustrates the utility of spatially resolved long slit observations. In this figure, wavelength increases along the x-axis, and the y direction shows spatial structure along the length of the long slit.

so it is straightforward to combine observations using the different channels. Two of these detectors are Multi-Anode Microchannel Arrays (MAMAs), while the third is a CCD.

Table 1: STIS Detectors

Detector	type	dimensions (pixels)	$\approx$ wavelength range (Å)	FOV ($''$)	plate scale ($''$)
FUV MAMA	CsI	1024×1024	1150 - 1700	25×24	0.025
NUV MAMA	Cs_2Te	1024×1024	1600 - 3200	25×24	0.025
CCD	SITe	1024×1024	1650 - 11,200	25×24	0.0507

A number of gratings can be used with each of these detectors, and for each grating a large number of apertures are available. The first order gratings provide resolutions that vary between $\approx$ 600 and $\approx$ 1400 (depending on mode and wavelength), while the echelle modes provide resolution between $\approx$25,000 and 114,000, although with special observing techniques, resolutions of up to 200,000 can be obtained with the STIS E140H and E230H echelle modes (e.g., Jenkins, & Tripp 2001).

Most commonly, the first order grating modes are used with the long slits, allowing spatially resolved spectroscopy (Fig. 1), while the echelle modes are used with small apertures to minimize the overlap between the multiple spectral orders projected onto the detector (Fig. 2).

1.1. STIS History

STIS was originally installed into *HST* on February 14, 1997 during *HST* Servicing Mission 2 (SM2). The initial on-orbit performance of STIS is detailed in Kimble et al. (1998)

The instrument operated using its primary Side-1 electronics until May 16, 2001 (42,000 hours), when a malfunction disabled the Side-1 electronics. This malfunction is believed to have been a hard short in a tantalum capacitor, and this failure rendered all of the Side-1 electronics unusable.

STIS resumed observations on July 7, 2001, using the redundant set of Side-2 electronics. There were two notable differences in the operation of STIS after the switch to Side-2.

One of these changes was the presence in the CCD channel of additional electronic read-noise in the form of a herringbone pattern with approximately 1 e^- RMS. The behavior of this additional read-noise and techniques for removing it are discussed by Jansen et al. 2003.

The STIS Side-2 electronics also lack the ability to measure the temperature of the STIS CCD detector. On Side-1, the thermo-electric cooler (TEC) was operated in a closed loop

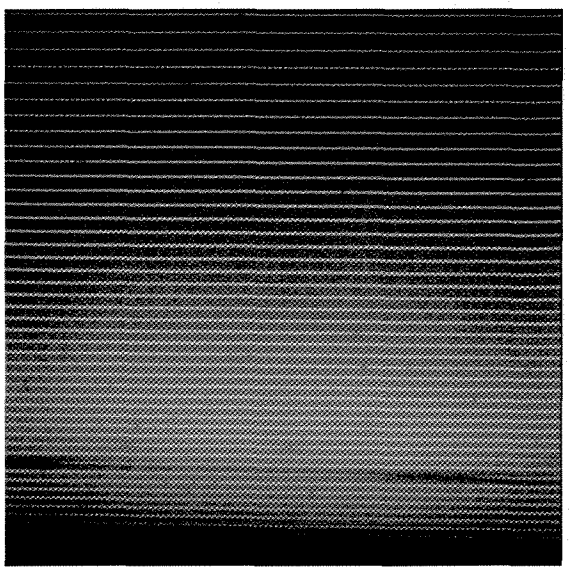

Figure 2: The flat fielded image for the STIS E140M echelle observation OB8709020 of the standard star BD+28° 4211 is shown using a logarithmic stretch. This figure illustrates the multiple spectral orders that can be simultaneously observed using the STIS echelle modes.

to maintain the detector at a constant set point of −83 C, but the lack of the appropriate sensor makes this impossible on Side-2. Instead, the TEC is operated at constant current, and the temperature of the CCD sensor fluctuates as the thermal environment of the aft shroud and the STIS instrument changes. These temperature fluctuations lead to significant variations in the detector dark current, including the brightness of hot pixels, on orbital time scales. However, there is a working sensor on the CCD housing, and it has proved possible to use this housing temperature to scale the dark current for these orbital variations (see Brown 2001 and Brown & Davies 2003). This scaling is applied in the STIS data reduction pipeline when constructing the STIS CCD dark reference files and when subtracting these reference darks from individual STIS CCD exposures.

Operations on Side-2 continued until August 3, 2004 (an additional 27,000 hours of operation), when a 5V power converter failed. The detectors were undamaged, but because this converter is necessary for the operation of essentially all the STIS instrument's moving parts, there was no way to adjust the gratings and apertures to allow light to reach the detectors.

Following the 2004 failure, a plan was conceived to replace the Side-2 circuit board containing the failed converter during *HST* Servicing Mission 4 (SM4). Technical details of the planned repair are described in Rinehart et al. (2008). On May 17, 2009, this repair was successfully carried out by astronauts Michael Good and Mike Massimino, and STIS was returned to operation. Since only the Side-2 electronics were repaired, the performance changes described above that are unique to Side-2 continue during the new post-SM4 period of operations.

2. Changes between 2004 and 2009

Most internal and external alignments, the overall focus, and the mechanical and electronic functioning of STIS are similar to that seen during previous side-2 operations. Some small zero-point offsets are compensated for by normal acquisition and wavecal procedures.

Significant fading of the STIS PtCr/Ne wavelength calibration lamps has been noted at the very shortest wavelengths (Pascucci et al. 2010ab). For a small number of STIS CENWAVE settings, the lamp choice and/or exposure times are being adjusted to compensate for these declines.

The STIS instrument does exhibit some degradation from its time on-orbit. Radiation damage is continuing to accumulate on the STIS CCD detector, resulting in increased dark current, more hot pixels, and increased effects from the decline in charge transfer efficiency. The throughput for most STIS channels showed modest declines after the hiatus, but not more than would have been expected from a simple extrapolation of previous trends.

The biggest surprise after STIS repair was the very high and slowly declining dark rate seen in the NUV MAMA detector.

Below we go into greater detail on some of these changes.

2.1. STIS CCD Performance

A detailed update on STIS CCD performance can be found elsewhere in these proceedings (Wolfe et al. 2010), so here we will concentrate on discussing the effects that these changes have on observers.

The herringbone pattern that appeared with the switch to the Side-2 electronics is still present with essentially the same characteristics and amplitude. However, the overall read-noise of the STIS CCD does appear to have increased by $\approx 0.3\,e^-$. This change appears to affect all gain setting and amplifiers, and unlike the herringbone noise does not appear to have a coherent pattern that would allow its removal via Fourier techniques.

The CCD dark rate has continued to increase, not only because of the accumulation of additional radiation damage, but also because temperatures inside STIS are higher than they were in the past due to the gradual degradation of *HST's* thermal insulation. In 2010, the average CCD housing temperature has been about 4 degrees C higher than it was in 2001. Given the observed 7%/degree dependence of the dark rate on the housing temperature, this effect alone results in a 31% increase in the dark rate.

Even after correction for the temperature variations, the CCD dark current after SM4 shows considerably more scatter than previously (Fig. 3). The causes of this additional scatter are currently under investigation.

For observations targeting faint objects, the most serious effect of radiation damage may be the "tails" that appear on hot pixels and cosmic rays. These are caused by the reappearance of charge from short time-scale traps. Effectively, some of the charge lags a bit behind during the CCD readout, i.e., the charge transfer efficiency (CTE) is < 1 and decreasing over time. The tail size and length increases with the number of charge transfers performed during the readout, so these effects increase dramatically with increasing distance from the readout register. These tails are obvious when looking at a typical STIS CCD dark reference file image (see the vertical streaks in Fig. 4; the readout register is along the top in this figure). Note that because CTE losses in the serial readout register are small, there are no tails visible along the rows (horizontal direction in Fig. 4).

Because of CTE effects, there is a significant decrease in the effective background and noise if the spectrum can be placed closer to the serial readout, especially for faint objects. To this end, special "E1" aperture positions along the long slit were defined to put the spectrum near row 900 of the detector; this reduces the number of parallel transfers during the readout by about a factor of 4. There are a few disadvantages to the E1 positions. Since they lie between the long slit fiducial bars and the top of the detector, there is a smaller unobstructed distance available along the slit. Also, there is some vignetting near the top of the detector, that varies between gratings, making the absolute flux calibration less certain. Finally, the quality of the G750L and G750M IR fringe flats for point sources at the E1 positions will not be as good. Near row 512, the 0.1x0.09 aperture can be used to provide fringe flats with a PSF very similar to that of point source observed in the long slit. If the

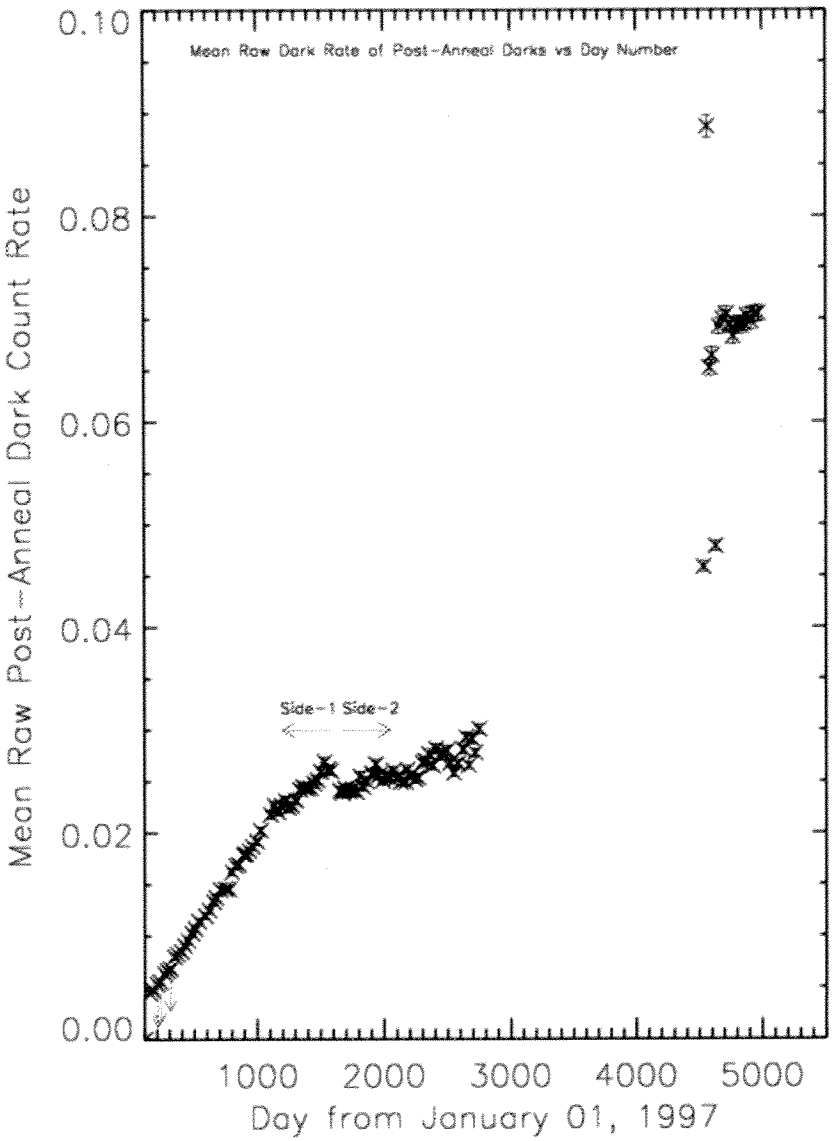

Figure 3: Median CCD dark rate after rejection of hot pixels as determined from monitoring observations throughout the on-orbit lifetime of STIS.

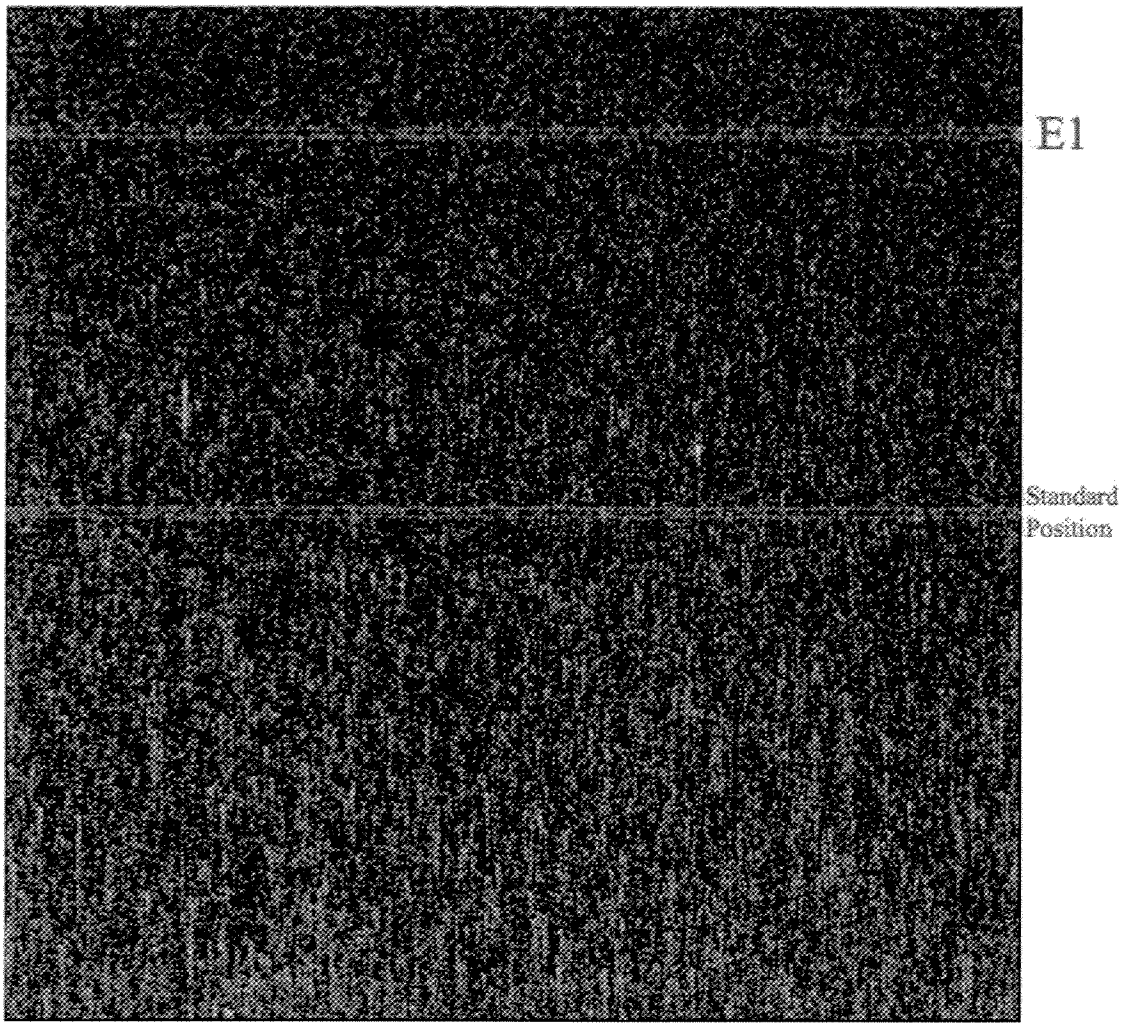

Figure 4: STIS CCD dark reference file.

slit wheel were to be simply rotated to put this aperture near row 900, the rotation of the slit wheel will have shifted it too far along the dispersion direction to allow the resulting fringe flat to be well aligned with the external spectrum.

2.2. Instrument Throughputs

The dependence of STIS throughputs as a function of time and wavelength have been tracked since 1997, using the same set of standard stars. The observed changes are believed to result from a combination of optical contamination (primarily organic molecules darkened by exposure to UV light) and possibly also some degradation of the detectors or small changes in the grating tilts. These time-dependent sensitivity (TDS) changes are monitored by periodic observations of selected standard stars. Results from before the 2004 STIS failure were summarized in Stys et al. (2004). While the detailed dependance at a given wavelength varies with channel, for a given detector, applying the degradation derived from the low-dispersion modes to the higher resolution gratings used with that detector has been an adequate approximation to past behavior.

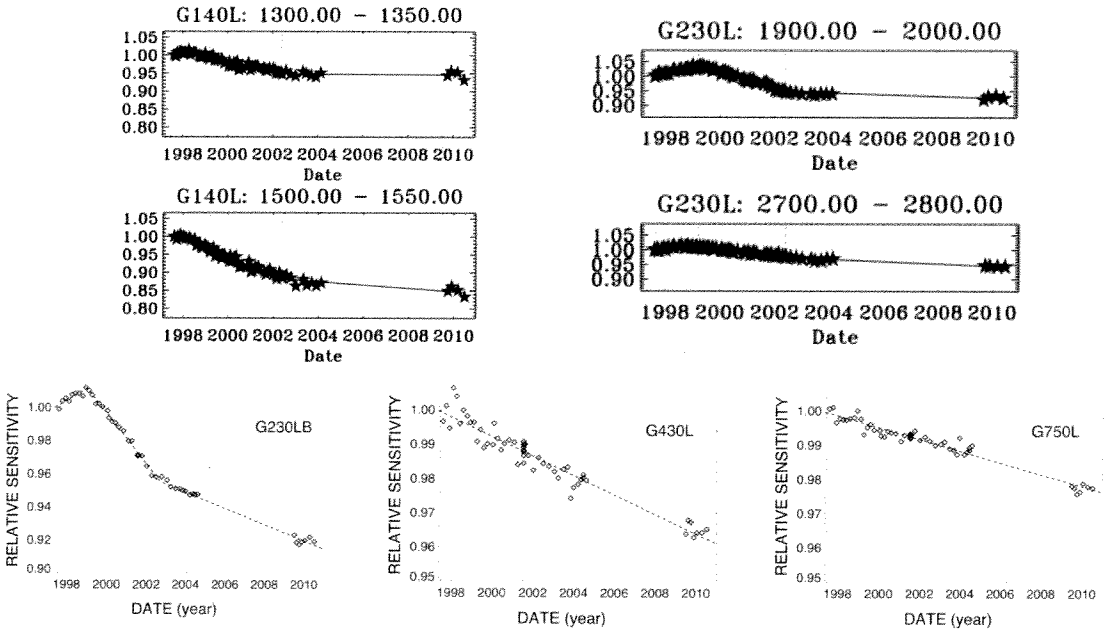

Figure 5: Time dependent changes in the throughput of STIS low dispersion modes.

Figure 5 shows the history of the time dependent sensitivity changes for a typical wavelength bin of each of the STIS low dispersion modes. The upper two panels show the results for the MAMA G140L and G230L gratings, while the lower three panels show results for the STIS CCD G230LB, G430L, and G750L gratings. Starting around 2002, the rate of decline of the STIS UV throughputs appears to have flattened, and degradation between 2004 and the post-SM4 period appears to be consistent with a simple projection of those trends. Further details are given in Osten et al. 2010.

The behavior of the STIS E140H grating may be a possible exception to the trends shown in Figure 5. This grating initially seemed to show substantially lower throughput (by 15 - 20 %) than a simple extrapolation of the previous trends would have suggested. However, the grating throughput appears to have recovered from this anomaly within a few months after SM4. Additional details of this behavior, along with a discussion of changes in the echelle blaze function alignment, can be found in Bostroem et al. (2010) elsewhere in these proceedings.

2.3. NUV MAMA Dark Rate

The dark rate seen by the STIS NUV MAMA detector is believed to be dominated by a phosphorescent window glow. A simple model for this glow was initially presented by Kimble (1997) and also by Jenkins (1997), and was further discussed by Ferguson & Baum (1999). Metastable states resulting from impurities in the window become populated by charged particle impacts; these states do not decay, but instead are depopulated by thermal transitions to unstable states, which produce the UV photons that cause the background. This process is illustrated in Figure 6. The need to thermally excite the meta-stable state to depopulate causes the dark rate over short time scales to be an exponential function of the window temperature. However, over longer time scales, keeping the detector window cold causes a large population of meta-stable states to build up, and when the detector is subsequently warmed back up, a large, but temporary, increase in the window glow results until a new equilibrium is reached. Based on pre-SM4 modeling, it had been expected that the dark rate would be initially enhanced by a factor of 2 to 3 above the pre-SM4 long term

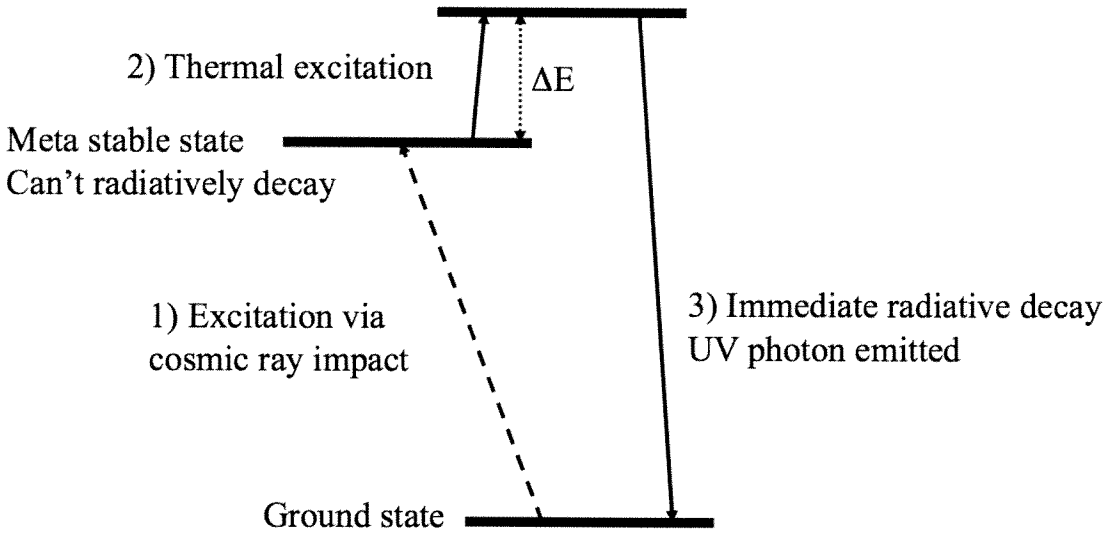

Figure 6: Schematic representation of the source of the NUV MAMA dark current.

equilibrium mean rate of about 0.0013 counts/pixel/s, but would come back to near that equilibrium rate within two to three weeks. Instead the dark rate was found to be as high as 0.015 counts/pixel/s, and the subsequent decline has been much slower than expected. As of fall 2010, the mean dark rate was about 0.0035 counts/s/pixel, about 2.5 times the rate seen in 2004, and the time scale for further decreases appears to very long. Additional details of the history of the STIS NUV MAMA dark rate, as well as a comparison with the COS NUV MAMA, can be found in Zheng et al. (2010) elsewhere in these proceedings.

3. Future Calibration Plans

Following the completion of the initial post-SM4 verification observations, the Cycle 17 STIS calibration program was initiated to perform monitoring and ongoing calibration of instrument performance and to fill in any gaps left by the initial calibrations. Full details of each Cycle's STIS calibration plan can be found at `http://www.stsci.edu/hst//stis/calibration/`.

In addition to the routine monitoring observations, there are a number of ongoing activities of particular note:

- Flux recalibration of all STIS echelle settings to allow shifts in the echelle blaze function to be determined – see Bostroem et al. (2010) and *HST* CAL/STIS program 11866 for further details.
- Improvements to CCD dark current scaling and subtraction are underway (see also Jansen et al. 2003 for a discussion of the STIS herringbone pattern noise). In the near future, we also hope to consider whether pixel-based corrections for charge transfer efficiency losses, similar to those being developed for ACS by Anderson & Bedin (2010), might also be usefully applied to STIS CCD detector data.
- New observations to determine the stability of the MAMA pixel-to-pixel flats and to derive new STIS CCD pixel-to-pixel flats (Niemi et al. 2010, and HST CAL/STIS proposals 11852, 11861, and 11862).
- Improvements to our understanding of STIS wavelength calibration lamp performance and dispersion relations (Pascucci et al 2010ab, and Ayres 2010).

4. Summary

Overall, the performance of STIS after its repair during SM4 is, in most ways, close to that seen during the previous period of operations between 2001 and 2004 using the Side-2 electronics. Most of the changes seen are indeed close to extrapolations of previous trends. It is hoped that STIS will remain an important part of *HST's* instrument complement for many years to come.

References

Anderson, J., & Bedin, L. R. 2010, PASP, 122, 1035

Ayres, T. 2010, these proceedings

Bostroem, K. A., Aloisi, A., Proffitt, C. R., Osten, R., & Lennon, D. 2010, these proceedings

Brown, T. M. 2001, Instrument Science Report STIS 2001-03, Temperature Dependence of the STIS CCD Dark Rate During Side-2 Operations (Baltimore: STScI)

Brown, T. M., & Davies, J. E., 2003, in Proc. 2002 *HST Calibration Workshop*, ed. S. Arribas, A. Koekemoer, & B. Whitmore (Baltimore: STScI), 180

Ferguson, H., & Baum, S, 1999, STIS Instrument Science Report 1999-02, "Scientific Requirements for Thermal Control and Scheduling of the STIS MAMA detectors after SM-3," (Baltimore: STScI)

Jansen, R. A., Collins, N. R., & Windhorst, R. A. 2003, in Proc. 2002 *HST Calibration Workshop*, ed. S. Arribas, A. Koekemoer, & B. Whitmore (Baltimore: STScI), 193

Jenkins, E. B. 1997, "A study of near-UV MAMA dark count rates: Modeling and predictions" private memo

Jenkins, E. B., & Tripp, T. M. 2001, ApJS, 137, 297

Kimble, R. A. 1997, "STIS IDT Post-Launch Quick-Look Analysis Report #37; Temperature/Time Modeling of MAMA2 Phosphorescent Dark Rate"

Kimble, R. A., et al. 1998, ApJ, 492, L83

Niemi, S., Proffitt, C. R., Ake, T., & Lennon, D. 2010, these proceedings

Osten, R., et al. STIS ISR in preparation, "Post-SM4 Sensitivities for the STIS MAMA Spectroscopic Modes", (Baltimore: STScI)

Pascucci, I., Proffitt, C., Ghavamian, P, Sahnow, D, Oliveira, C, Aloisi, A, Keyes, T, & Penton, S. V. 2010a, Proceedings of the SPIE, 7731, in press

Pascucci, I., Proffitt, C., Ghavamian, P, Sahnow, D, Oliveira, C, Aloisi, A, Keyes, T, & Penton, S. V. 2010b, these proceedings.

Rinehart, S. A., et al. 2008, Proceedings of the SPIE, 7010, 138

Stys, D. J., Bohlin, R. C., & Goudfrooij, P. 2004, STIS Instrument Science Report 2004-04, "Time-Dependent Sensitivity of the CCD and MAMA First-Order Modes" (Baltimore: STScI)

Wolfe, M. et al. 2010, these proceedings

Zheng, W. et al. 2010, these proceedings